

## *Scientific Report 2013-2015*

### **Ideas program. Exploratory research projects**

Implementation of project Cod PN-II-ID-2012-4-0028:  
**Alkali and silver halides based magnetic tunnel junctions**  
*January 2016- September 2016*

#### *2016 Year report*

##### **Objectives for 2015 and 2016:**

- I. Fe/LiBr(001) and Fe/LiF(001) junctions**
- II. Fe/NaBr/Fe(001) interfaces**
- III. Double perovskites based on calcium**

**Expected Results:** publication of two or three papers in ISI quoted journals. Presentation of one paper at International conference.

##### **Report content:**

- I. Fe/NaBr/Fe and Fe/AgBr/Fe interfaces**
- II. Transport properties of Fe/Na<sub>1-x</sub>Ag<sub>x</sub>Br/Fe magnetic tunneling junctions**
- III. Crystal structures and magnetic properties of Ca<sub>2</sub>(Fe,Ni)MoO<sub>6</sub> double perovskites**
- IV. Rare earth compounds of RCo<sub>2</sub>-type**

##### **Report:**

- I. Fe/NaBr/Fe and Fe/AgBr/Fe interfaces**

Ground state self-consistent electronic structure calculations on the rocksalt (Fm3m) NaBr and AgBr compounds were performed by using the standard tight-binding linear muffin-tin orbital (TB-LMTO) method in the atomic sphere approximation. All calculations were performed in the scalar-relativistic limit, i.e. without spin-orbit coupling. The Vosko-Wilk-Nusair parameterization was employed for the exchange-correlation energy, within the local density approximation (LSDA). Due to the non-closed-packed structure of the rocksalt-type structure, two empty spheres (ES) were inserted at the appropriate interstitial positions between NaBr(AgBr) layers, without breaking the crystal symmetry.

The band structures of NaBr and AgBr compounds are given in Fig.I.1. The computed band gaps are of 3.6 eV (NaBr) and 0.9 eV (AgBr). These values are somewhat smaller than those experimentally determined.

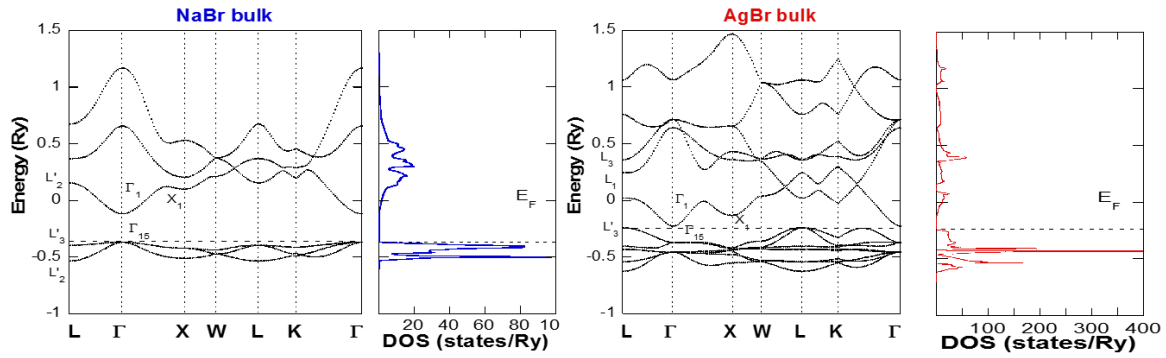


Fig.I.1

The structures of Fe/NaBr(AgBr)/Fe junctions are given in Fig.I.2. The calculations were made at lattice parameters epitaxially fixed at lattice spacing of iron,  $a_{\text{NaBr}} \cong 2 a_{\text{Fe}}$ ,  $a_{\text{AgBr}} \cong 2 a_{\text{Fe}}$ . The NaBr and AgBr epitaxially fit the bcc Fe structure. Two model interfaces were analysed:

- C1, where Fe atoms are located atop of Ag(Na) and Br positions.
- C2, where Fe atoms are located above the hollow sites, between Na(Ag) and Br sites.

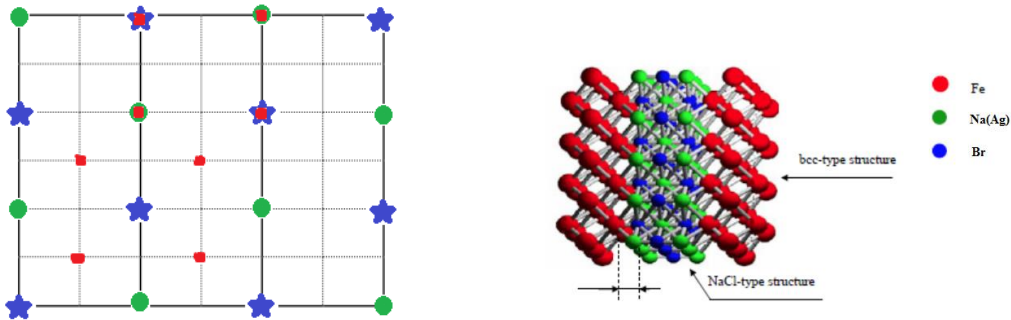


Fig.I.2

In order to fulfill ASA space filling, at the Fe/NaBr(AgBr) interfaces, two empty spheres were introduced. Due to empty sphere planes located between adjacent NaBr(AgBr) layers, the spacers are non-symmetric. In order to have symmetric junctions (with even number of monolayers), non symmetric electrodes with  $n$  and  $n+1$  iron layers were considered. Thus, as example, the calculations were made on 6Fe/9NaBr/7Fe junctions. The atomic monolayers were denoted by I, I-1, I-2, ... in the magnetic slab and I, I+1, I+2... in the barrier.

The ground state electronic structures and magnetic properties of 6Fe/9NaBr/7Fe junctions, as determined from present calculations, are plotted in Fig. I.3. Due to location of the iron Fermi level near the bottom of the NaBr conduction band, there is a charge transfer between iron magnetic slabs and NaBr spacers. The result of the charge transfer, at interfaces, is the formation of Metal Induced Gap States (MIGs) in the band gap of the barrier. Away from the

interfaces the iron layers recover the bulk like charge distribution, whilst the NaBr barrier tends to recover it even from the second layer from Fe/NaBr(001) interface. At the C1 interface, the charge transfer of iron is of  $\cong 0.77 e^-$ , but smaller at C2 interface, of  $\cong -0.38 e^-$ . On the barrier side, at C1 interface, the Br charge decreases by  $\cong 0.03 e^-$  and at the Na by  $\cong 0.02 e^-$ . At the C2 interfaces the charges of both Br and Na increase by  $\cong 0.22 e^-$  and  $0.55 e^-$ , respectively – Fig.I.3.

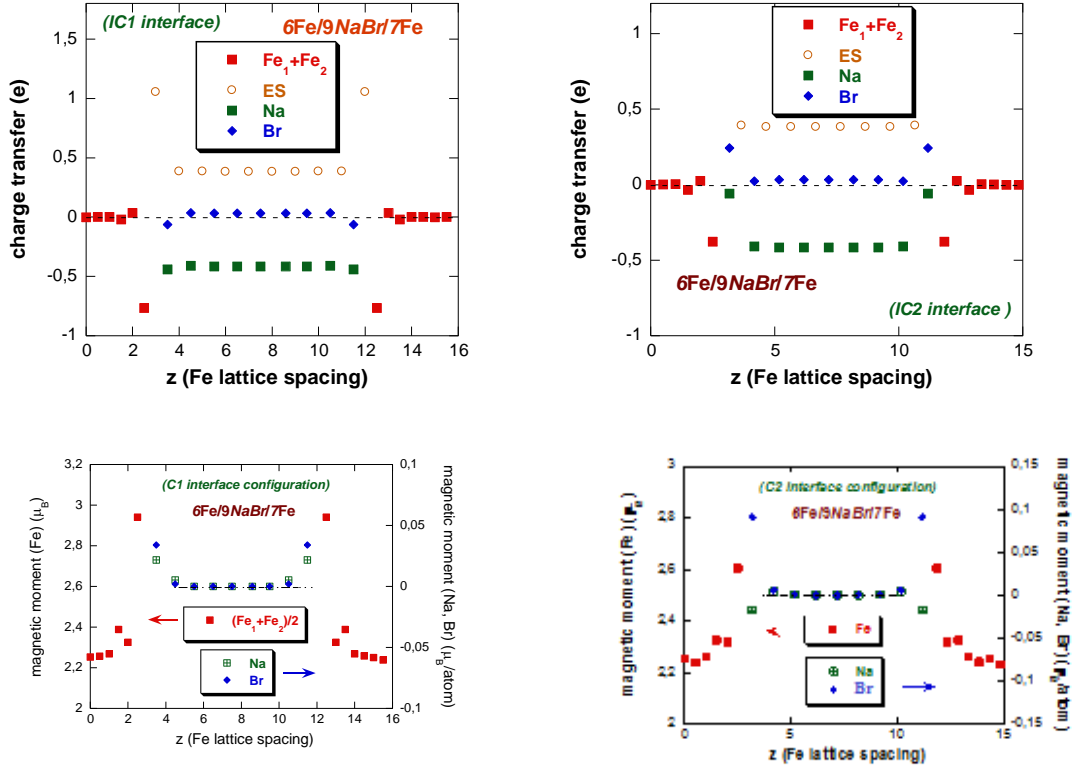


Fig.I.3

The interfacial iron moments, both at C1 and C2 interfaces, are enhanced over the bulk values, being of  $\cong 2.94 \mu_B$  and  $\cong 2.60 \mu_B$ , respectively. According to notations on Fig.I.3, small polarizations are induced on Na ( $\cong 0.02 \mu_B$ ) and Br ( $0.03 \mu_B$ ) in the layers with  $z = 3$  and  $12$ , at C1 interface. Inside the barrier ( $4 \leq z \leq 11$ ), both Na and Br are not polarized. At C2 interface, the induced polarizations, on the same layers as above ( $z = 3$  and  $12$ ), are negative for Na ( $\cong -0.02 \mu_B$ ) and positive for Br ( $\cong 0.09 \mu_B$ ). Inside the barrier no polarizing effects were shown.

The layer and atom-resolved spin-polarized DOS of 6Fe/NaBr/7Fe junction has been also studied – Fig. I.4. The DOS of iron away from C1 interface (I-2), is of bulk like type with partially filled majority-spin 3d sub-band. The Fermi level,  $E_F$ , is located at a dip in the minority-spin 3d sub-band. At interface (FeI), the DOS is modified, due to lower coordination number of Fe atoms and also due to interaction with NaBr interfacial layer. Thus, the minority spin band is nearly fully occupied and the majority spin band nearly empty.

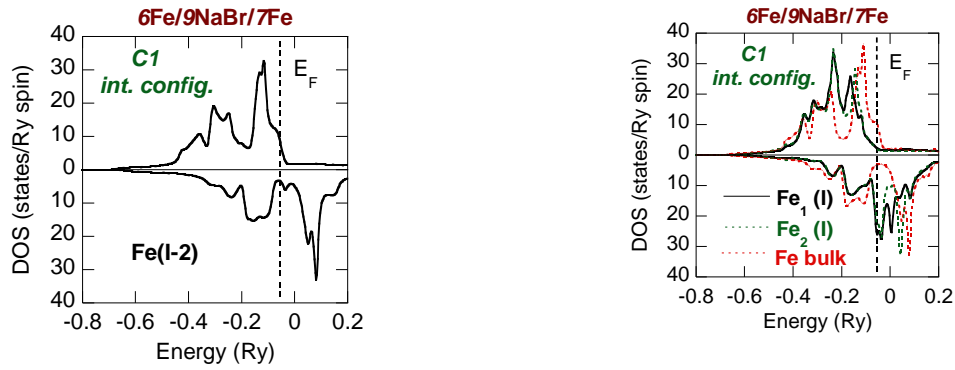


Fig.I.4

Iron metal induced gap states were evidenced in NaBr barrier near the interfaces at both Na and Br – Fig.I.5. Thus, the Fe/NaBr(001) interfaces are partially metallic. Departing from interfaces the isolating character is recovered. At induced gap states, contribute the d, p and s electrons.

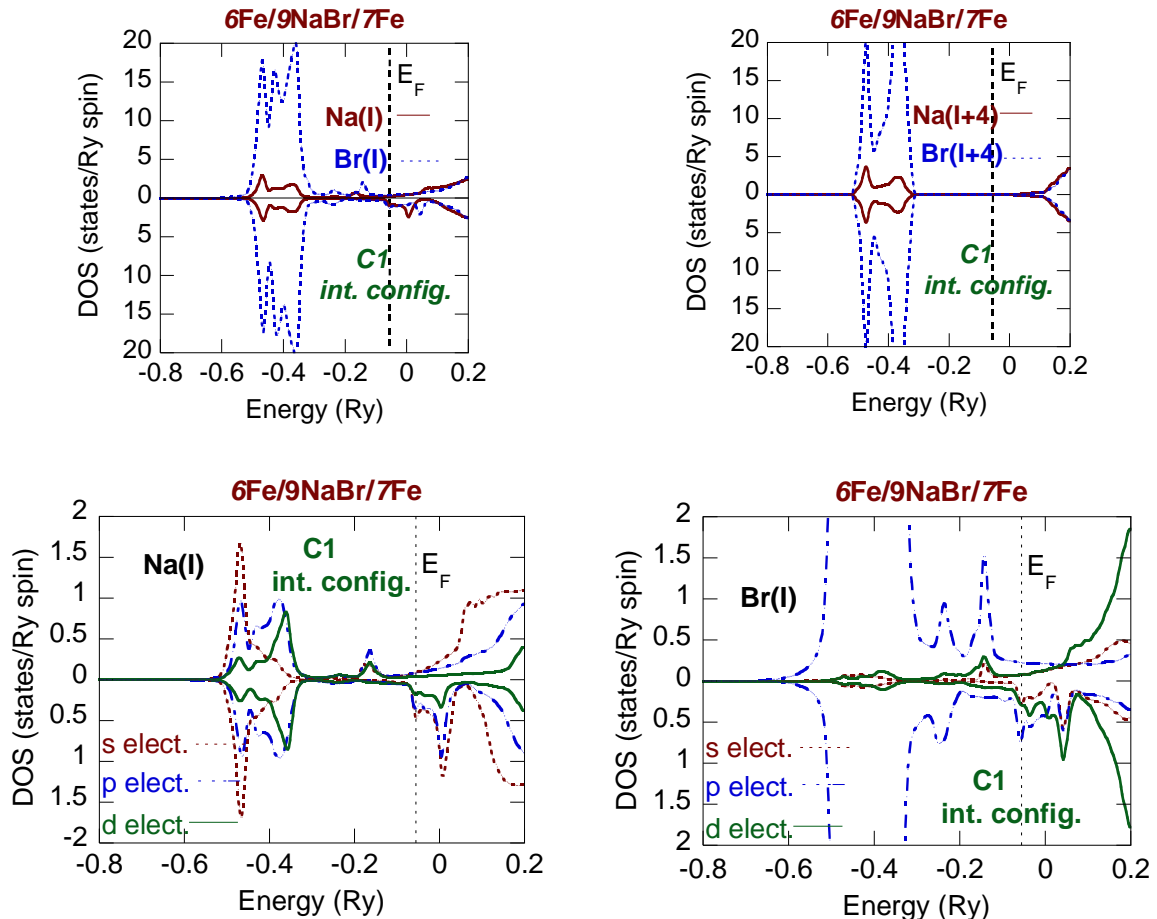


Fig.I.5

The interlayer exchange couplings in 6Fe/mNaBr(AgBr)/7Fe heterojunctions were studied – Fig.I.6. In case of NaBr barrier, at C1 interface, the exchange coupling between

Fe(001) slab and the NaBr spacer is small and positive for  $3 \leq m \leq 8$  and negative at C2 interface from  $m \leq 6$ . The exchange coupling decays exponentially with barrier thickness.

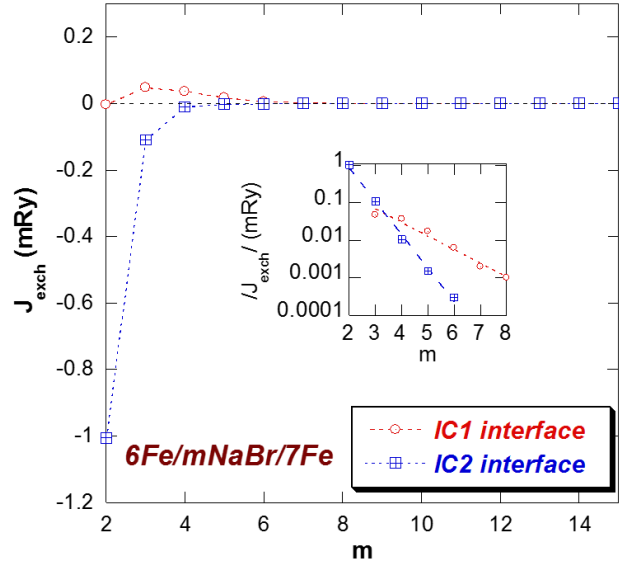


Fig.I.6

Generally, the interlayer exchange coupling is negative if  $k_F^2 < k_F^\uparrow k_F^\downarrow$  and positive when  $k_F^2 > k_F^\uparrow k_F^\downarrow$ . By  $k_F$  is denoted the wave vector in the barrier and  $k_F^\uparrow, k_F^\downarrow$ , the wave vectors in the magnetic electrode (iron). The  $k_F$  depends on the barrier height,  $k_F^2 \propto \sqrt{U_{\text{eff}}}$ . The observed behaviour, above mentioned, can be correlated with the barrier height which is high at C1 interface and small at C2 interface.

In the case of AgBr barrier, the interlayer exchange couplings both at C1 and C2 interfaces are oscillatory – Fig.I.7. The oscillatory behaviour can be related to large amount of MIGs near the interface. The damped oscillations are related to small barrier height.

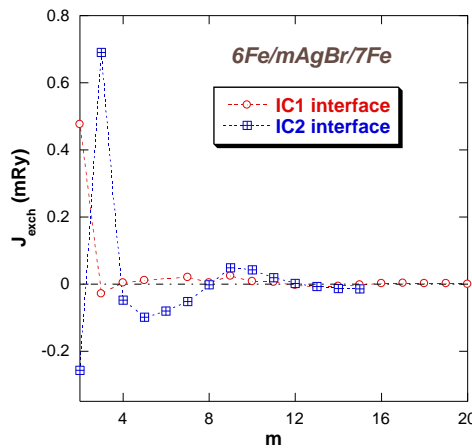


Fig.I.7

The spin dependent transport properties of 6Fe/mNaBr/7Fe junctions were studied – Fig.I.8. The conductances exponentially decay with the barrier thickness. The dominant contribution to transport properties, in case of C1-type interface, is evidenced for the ferromagnetic (FM) configuration with spin down electrons. A change in slope is evidenced at  $m = 8$ . In case of C2 interface, the same contributions to conductances, for all spin channels, are evidenced.

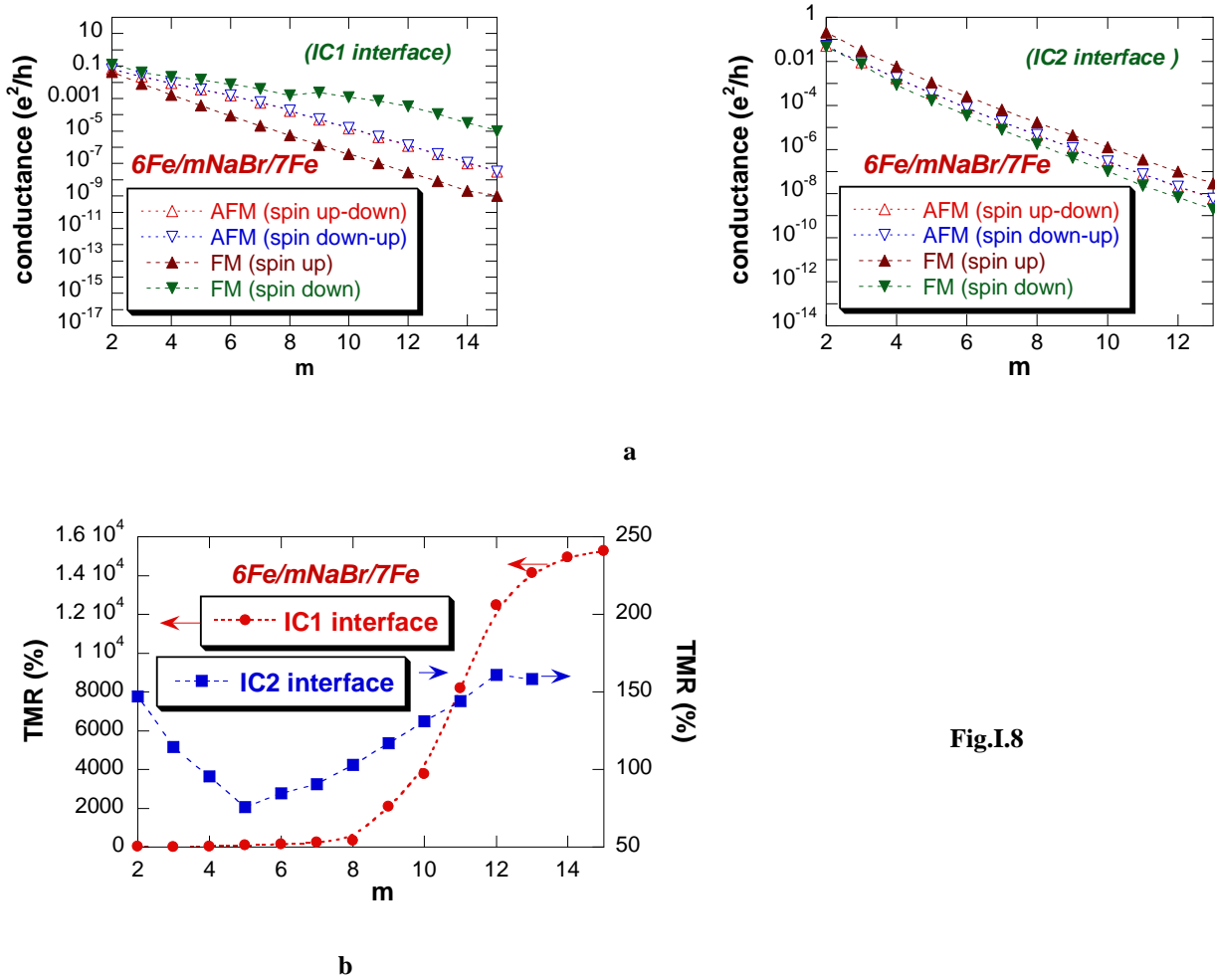


Fig.I.8

The tunneling magnetoresistance in case of C1 interface is very high, of  $\cong 10^4$  %, for  $m > 11$ , while when C2 interface is considered, this is of order of  $\cong 10^2$  – Fig.I.8b

The  $k_{||}$ -resolved conductances were also analysed. The transmission across a planar junction can be described considering the complex band structure of the barrier. At the interface, the wave vector is split in  $k_{||}$  component which is conserved during scattering and  $k_z$  along the transmission direction. Inside the barrier band gap,  $k_z = q+i$ , where the imaginary part  $i$  describes the exponential decay of the corresponding evanescent states. The transmission probability, for  $k_{||}$ , decreases exponentially with barrier thickness,  $d$ ,  $T \propto \exp(-2 kd)$ . The

exponentially decay of conductances, in the asymptotic region, confirms the presence of tunneling process across the NaBr(AgBr) barriers.

In the case of majority spin (spin up) conductances, the FM one is of free electron-like, with broad and large transmission maximum at  $\Gamma$  point – Fig.I.9. The conduction is determined by the  $\Delta_1$  states. In case of NaBr, the conduction band minimum, at the center of Brillouin zone, occurs at  $\Gamma_1$  point, while the top valence band at the  $\Gamma_{15}$  point – Fig.I.1. Thus, the bottom of the conduction band and the top of valence band will be connected by purely imaginary band with  $\Delta_1$  symmetry. There is a lower  $\Delta_1$  decay parameter. States with other symmetries than above mentioned, decay much faster and have negligible contribution to tunneling process. Thus, the  $\Delta_1$  channel is the only direct tunneling channel across NaBr(AgBr) barrier.

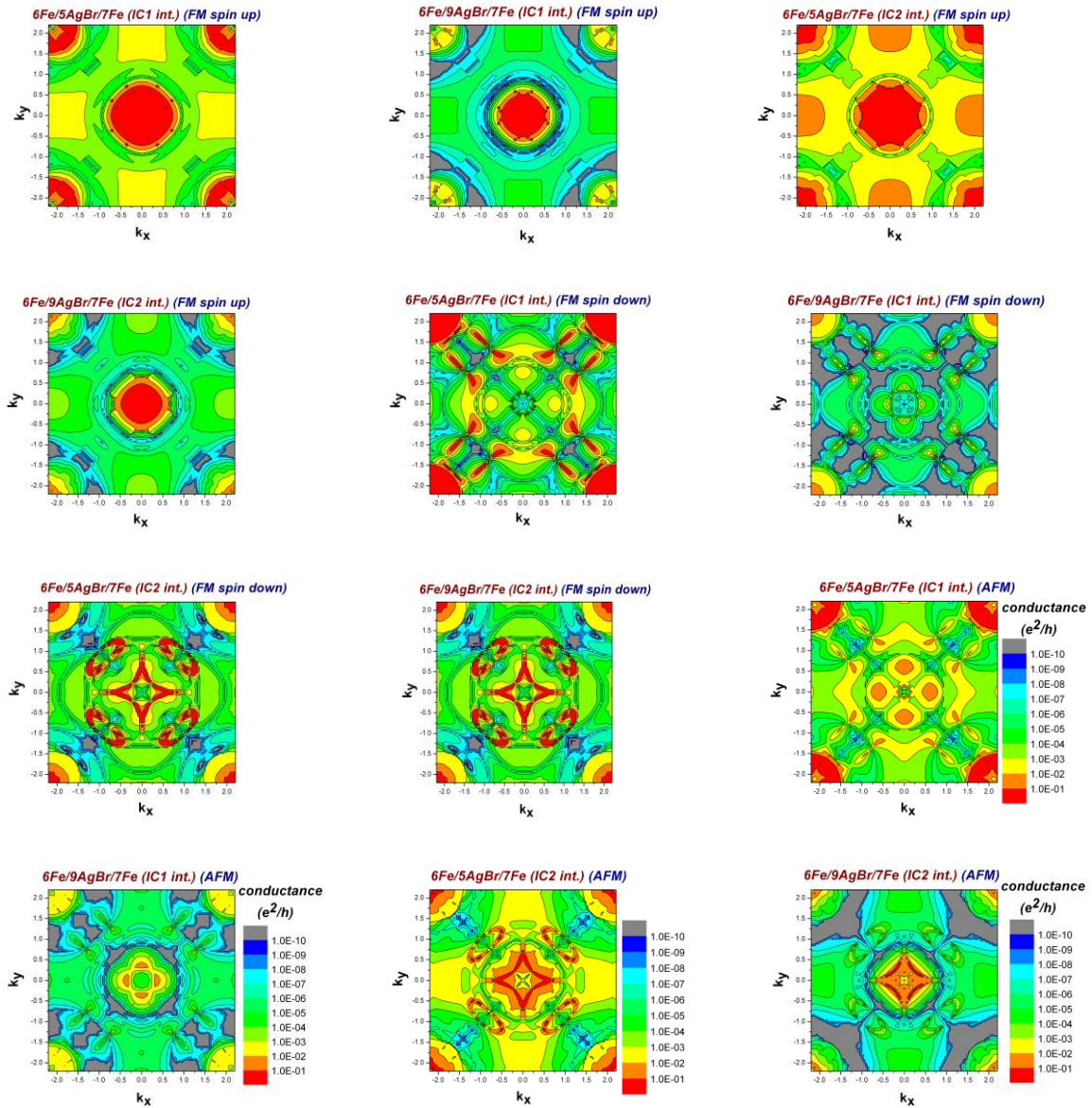


Fig.I.9

The minority-spin FM and AFM conductances are dominated by hot-spots or spike-like peaks around  $\bar{\Gamma}$  point – Fig.I.9. The spikes originate from the minority-spin interface resonant states and contribute to the increase of the transmission by resonant tunneling.

The large magnetoresistance ratios, above  $10^4$  %, in the C1 barrier configuration, makes this system attractive in the context of spin electronics.

## II. Transport properties of Fe/Na<sub>1-x</sub>Ag<sub>x</sub>Br/Fe magnetic tunneling junctions

The effect of variable content of Na and Ag in the NaBr barriers on the transport properties of 6Fe/9(Na<sub>1-x</sub>Ag<sub>x</sub>Br)/7Fe heterojunctions were studied. The analysis has been made in the case of C1-type interfaces.

The evolution of conductances as function of barrier composition is given in Fig. II.1. The FM conductances within spin down channel dominates for  $x < 0.2$  and those spin up at  $x > 0.8$ . In the intermediate region, near the same contributions are evidenced for both spin down and spin up electrons.

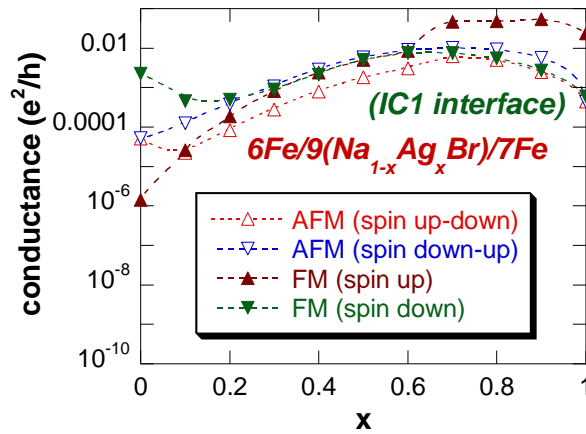


Fig.II.1

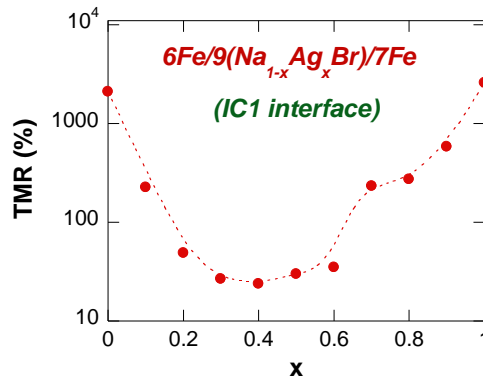


Fig.II.2

The composition dependence of the tunneling magnetoresistance is given in Fig.II.2. TMR values higher than 10<sup>3</sup> % has been evidenced for compositions with x = 0 and 1. These decrease in the intermediate composition region.

The scientific results obtained in the studies of heterojunctions were published in the international journals or presented at international conferences:

**I.1. *Are insulating LiF barriers relevant for spin-polarized tunneling applications?***

***Insights from first principles calculations***

**P. Vlais, E. Burzo, K. Carva**

*J. Phys.D: Appl. Phys.* 49, 305302 (2016) IF = 2.772

**I.2. *Spin-polarized transport using do ferromagnetism: an ab initio study of CaC/MgS/CaC(001) heterojunctions***

**P. Vlais, E. Burzo, K. Carva**

*J. Phys. D.: Appl. Phys.* 48, 455002-455010, 2015 IF = 2.772

**I.3. *Magnetic and electronic transport properties of some tunnel junctions with AgBr spin filter barrier***

**P. Vlais, E. Burzo**

*J. Phys.: Cond. Matter, (will be send for publication)*

Papers presented at international conferences:

**I.1. *Spin polarized transport properties in Fe/NaBr(001) based heterojunctions***

**E. Burzo, P. Vlais**

*Invited lecture, 16<sup>th</sup> International Balkan Workshop on Applied Physics, July 2016, Constanta, Paper SIL2 p. 12*

**I.2. *Spin dependent transport properties in MTJs having NaBr(AgBr) barriers***

**P. Vlais, E. Burzo**

*Poster paper, 11<sup>th</sup> International Conference on Physics of Advanced Material, 2016 p.309 Poster paper T4-P14*

**III. Double perovskites based on calcium**

**Crystal structures and magnetic properties of Ca<sub>2</sub>(Fe,Ni)MoO<sub>6</sub> double perovskites**

**III. 1 Crystal structures**

The Ca<sub>2</sub>Fe<sub>1-x</sub>Ni<sub>x</sub>MoO<sub>6</sub> double perovskites crystallize in a monoclinic structure having space group P2<sub>1</sub>/n, as evidenced in Fig.III.1. The lattice parameters increase as the nickel content is higher – Fig. III.2. This behaviour can be correlated with the greater Ni<sup>2+</sup> ionic radius (0.69 Å), as compared with those of Fe<sup>3+</sup> (0.645 Å) or Fe<sup>2+</sup> (0.61 Å) ions, situated in 6-coordination, Their cell volumes increase linearly, when increasing nickel content. The

monoclinic angle is close to  $90^\circ$ , indicating a strong pseudo-orthorhombic character of the unit cell. The antisite content, determined by XRD, increases nearly linearly with nickel content from  $\cong 6.6\%$  ( $x = 0$ ) up to  $9.5\%$  ( $x = 0.2$ ).

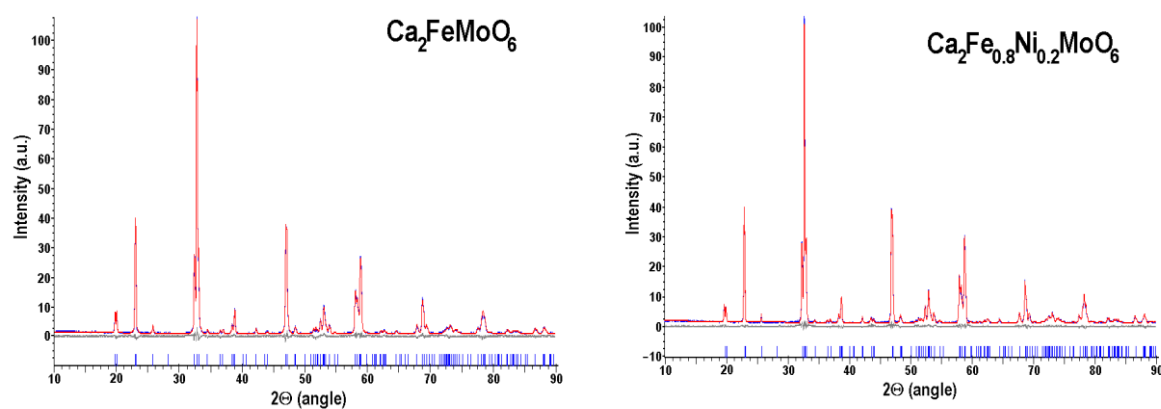


Fig.III.1

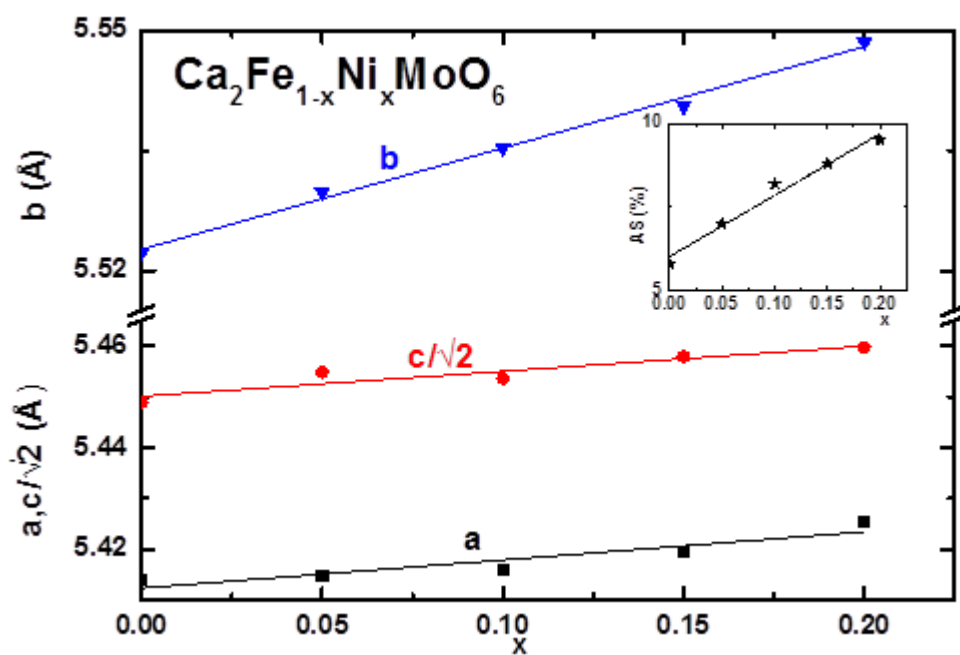
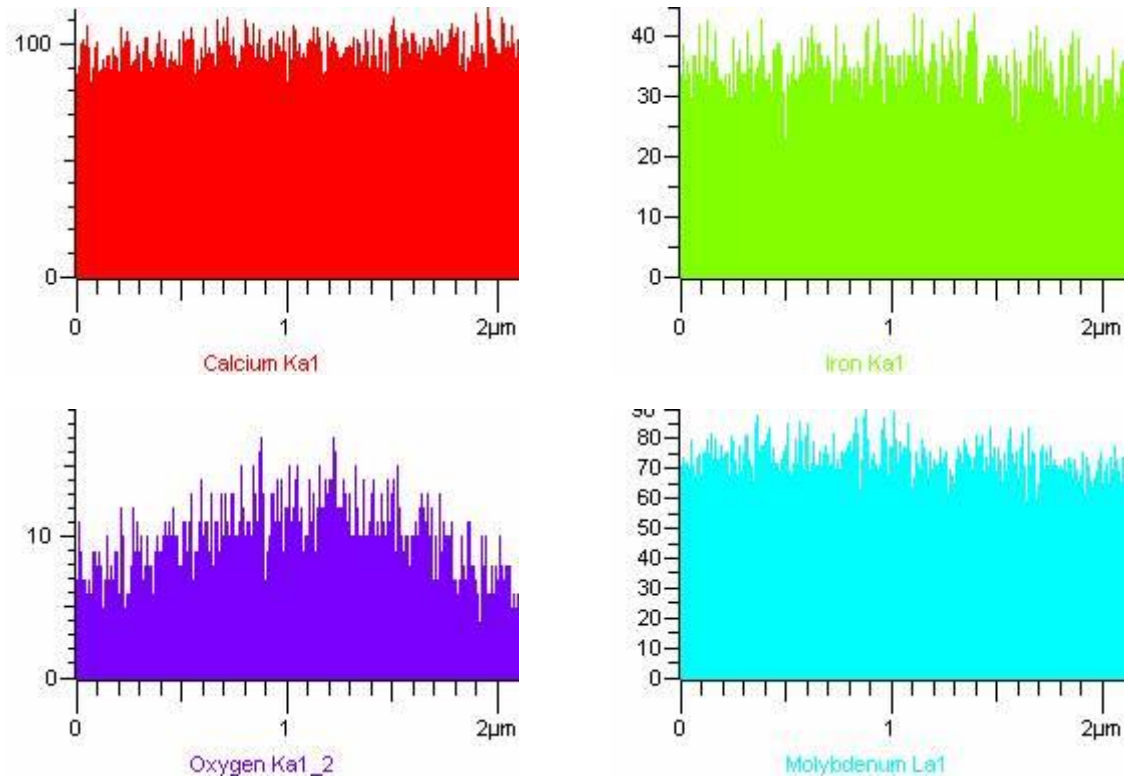


Fig.III.2



**Fig.III.3**

The samples compositions and grain dimensions were determined by SEM and EDS measurements. As example in Fig. III.3 are given the data obtained for the  $\text{Ca}_2\text{FeMoO}_6$  perovskite. There are some differences in the sample compositions as compared with the starting mixtures – Table III.1.

**Table 1**

**Magnetic properties**

x	Composition	$T_c$ (K)	$1/\chi_0$ (emu/f.u.) <sup>-1</sup>	C (emuK/f.u.)	$\sigma$ (emu/f.u.) <sup>-1</sup> K	$\theta$ (K)
0.1	$\text{Ca}_2\text{Fe}_{1.02}\text{Mo}_{0.955}\text{O}_{5.92}$	367	-96.4	3.67	520	331
0.2	$\text{Ca}_2\text{Fe}_{0.922}\text{Ni}_{0.09}\text{Mo}_{1.02}\text{O}_{6.1}$	330	-91.3	3.51	112	322
0.3	$\text{Ca}_2\text{Fe}_{0.81}\text{Ni}_{0.185}\text{Mo}_{0.99}\text{O}_{6.06}$	323	-97	3.21	84	311

The variable valence fraction of normalized calcium perovskites compositions can be described by the  $\text{Fe}_u^{3+}\text{Fe}_{1-u}^{2+}\text{Mo}_v^{5+}\text{Mo}_{1-v}^{6+}$  formula. Starting from the determined compositions by EDS method, according to charge neutrality condition, the u and v parameters were shown to be related:

$$u-v = 0.1 \text{ (} x = 0 \text{)}, 0.056 \text{ (} x = 0.1 \text{)}, 0.17 \text{ (} x = 0.2 \text{)} \quad (1)$$

### III.2 Magnetic properties

The temperature dependences of the magnetizations in zero field cooled (ZFC) and 1 kOe field cooled (FC) samples, having nominal compositions  $x = 0, 0.1$  and  $0.2$  are given in Fig.III.4. There are some small irreversibilities, suggesting the presence of a clusters glass contribution to the magnetizations. The magnetic moments of the clusters are aligned parallelly to external fields, for field intensities higher than 20 kOe. The saturation magnetizations at 4 K, decrease with a slope of  $\cong 0.7 \mu_B$  per substituted nickel atom. The perovskites are ferrimagnetically ordered.

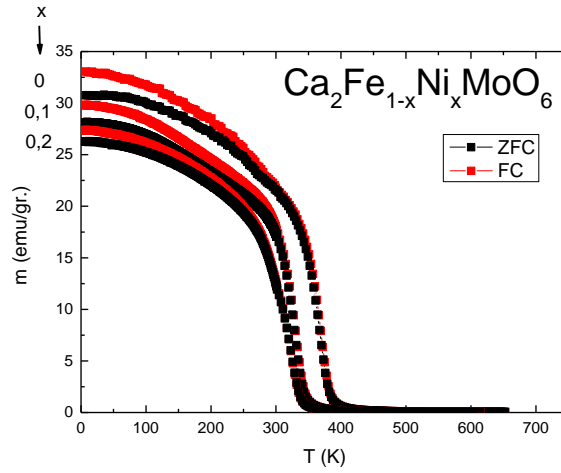


Fig.III.4

The magnetic data were analysed supposing that the ordered magnetic moments of ferric, ferrous and nickel ions are of  $5 \mu_B$ ,  $4 \mu_B$  and  $2 \mu_B$ , respectively. The most reliable value for  $\text{Mo}^{5+}$  moment is of  $0.32 \mu_B$ , as determined by X-ray magnetic circular dichroism.

The thermal variations of reciprocal susceptibilities show non-linear behaviour, characteristic for ferrimagnetic ordering – Fig. III.5. A two sublattices model, corresponding to B and B' sublattices magnetizations was assumed, in order to analyse the experimental data. In this model the temperature dependences of the magnetic susceptibilities can be described by the Néel relation:

$$\frac{1}{\chi} = \frac{1}{\chi_0} + \frac{T}{C} - \frac{\sigma}{T-\theta} \quad (2)$$

By C is denoted the Curie constant and the  $\chi_0^{-1}$ ,  $\sigma$  and  $\theta$  parameters are related to exchange interactions constants inside and between magnetic sublattices – Table III.1.

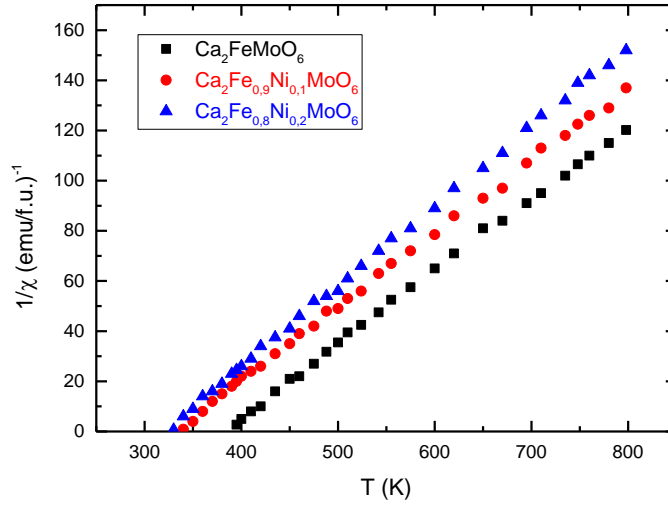


**Fig.III.5**

The Curie constants,  $C$ , determined in the asymptotic temperature range ( $T > 400$  K), decrease, as the nickel content is higher. Assuming an ionic model, where the Curie constants of the constituting elements are given by their free ions values, according to addition law of magnetic susceptibilities we have:

$$C = uC_{\text{Fe}^{3+}} + (1-u)C_{\text{Fe}^{2+}} + vC_{\text{Mo}^{5+}} \quad (3)$$

Starting from the relations (1) and (3), the distributions of the constituting ions, in different valence states, were determined. The number of ferrous ions decrease by  $\cong 21$  %, in the studied composition range, close to expected value of 18.5 %, as evidenced by the EDS study in the sample with  $x = 0.2$ . The content of ferric ions seems to be little affected when changing perovskites compositions. The valence states of molybdenum ions have been shown to be modified mainly due changes in oxygen content associated with samples compositions.

Starting from the determined saturation magnetizations and the antisite content, determined by XRD, the locations of the constituting ions in B and B' sites have been determined – Fig. III.6. The  $\text{Fe}^{3+}$  content in B' site is relative constant, and of 7-8 % in agreement with the antisite content as determined by XRD. A decrease of the number of  $\text{Fe}^{2+}$  ions in B site, parallelly with increasing nickel content is also evidenced.

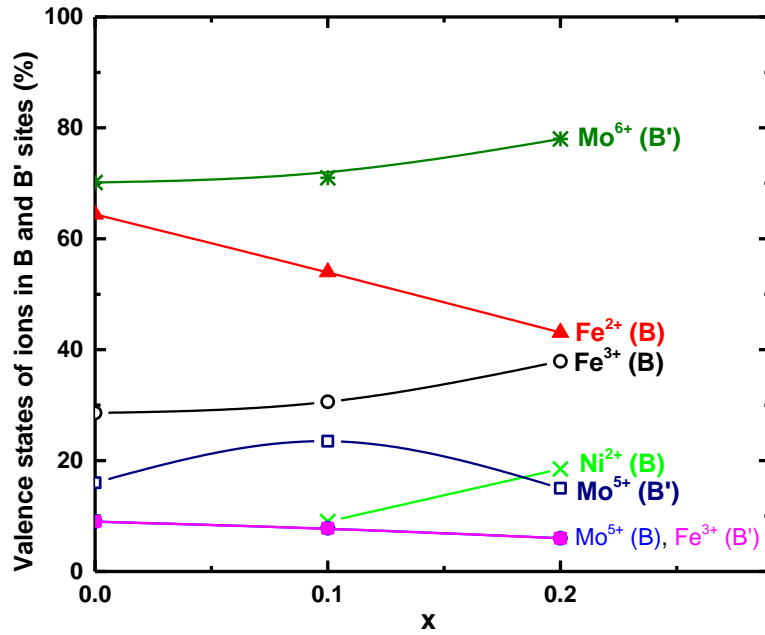


Fig.III.6

The exchange parameters (addimensional) characterizing the interactions inside ( $\alpha$ ,  $\beta$ ), as well as between magnetic sublattices ( $n$ ), were determined by using the mean field model – Fig.III.7. The  $n$  values are negative and decrease in absolute magnitude, correlated with magnetic dilution, as result of composition changes. The exchange interactions inside the magnetic sublattices increase as effect of substitutions.

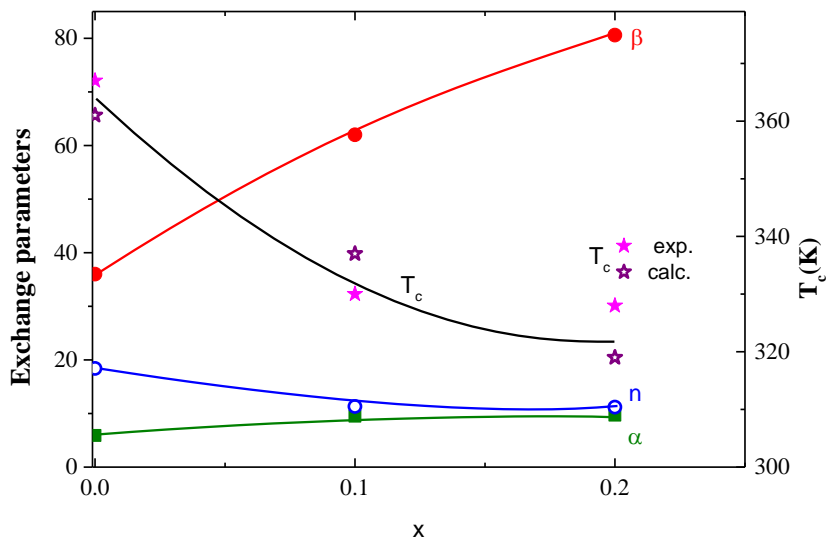


Fig.III.7

The consistency of the above data has been confirmed when these are used to compute the Curie temperatures according to Néel model. When using the determined exchange

interactions parameters, from paramagnetic data, the Curie temperatures are very close to those experimentally determined. The differences are of the order of only 1-2 %.

We conclude that the  $\text{Ca}_2(\text{Fe,Ni})\text{MoO}_6$  system shows mainly a ferrimagnetic type behaviour with a small cluster glass component. The magnetic properties both in magnetic ordered and paramagnetic ranges are well described when using a two sublattices mean field model. The spin polarization at  $T = 10$  K, is of 41 % in the perovskite with  $x = 0$ .

#### **Papers in the perovskite field published in 2016 year:**

##### **III.1. *Structural and magnetic properties of $\text{Ca}_{1.5}\text{La}_{0.5}\text{FeMoO}_6$ perovskites at high pressures***

**E.Burzo, D.P.Kozlenko, N.T.Dang, S.E.Kichanov, N.O.Golosova**

*Journal of Alloys and Compounds* 664, 363 (2016)

ISI journal IF = 3.014

##### **III.2. *Crystal structures, magnetic and transport properties of calcium based perovskites***

**E.Burzo, I.Balasz**

*AIP Conf. Proc.* 1722, 080003 (2016)

ISI journal

##### **III.3. *Ferrimagnetic order in $\text{Ca}_2(\text{Fe,Ni})\text{MoO}_6$ perovskites***

**E.Burzo, I.Balasz**

*Rom. J. Phys.* (2017) accepted for publication ISI journal, IF = 1.3

#### **Paper presented at international conference:**

***Magnetic properties of  $\text{Ca}_2\text{Fe}_{1-x}\text{Ni}_x\text{MoO}_6$  perovskites***

**I.Balasz, E.Burzo**

*11th International Conference of Physics of Advanced Materials, Sept. 2016, p. 90*

*Poster paper*

#### **IV Rare earths compounds of $\text{RCO}_2$ -type**

##### **IV.2 Magnetic and magnetocaloric properties of $\text{Er}_{1-x}\text{Y}_x\text{Co}_2$ compounds**

The  $\text{Er}_{1-x}\text{Y}_x\text{Co}_2$  compounds with  $x \leq 0.3$  crystallize in a cubic type structure, having  $\text{Fd}3\text{m}$  space group. The lattice parameters increase linearly, as the yttrium content is higher.

The magnetization isotherms obtained for the compounds with  $x = 0$  and  $0.2$  are plotted in Fig.IV.1. The magnetic moments, at 4 K, indicated that the compounds are ferrimagnetically ordered. The thermal variations of magnetic susceptibilities, are non linear as expected when a ferrimagnetic type ordering is present – Fig. IV.2. According to additivity law of magnetic susceptibilities and assuming that effective erbium moment is given by their free ion values, the effective cobalt moments,  $M_{\text{eff}}(\text{Co})$ , were determined. Both the Curie temperatures, saturation cobalt moments and the corresponding effective cobalt moments decrease as the

erbium is gradually replaced by yttrium – Fig.IV.3. Starting from the effective cobalt moments and the saturation ones, the number of spin  $S_p$  and  $S_0$ , characterizing the magnetic behaviour of cobalt in the two temperature ranges ( $T > T_c$  and  $T < T_c$ ) were determined. The ratio  $S_p/S_0$  follows  $T_c^{-2/3}$  dependence on Curie temperatures, as predicted by the spin fluctuations model.

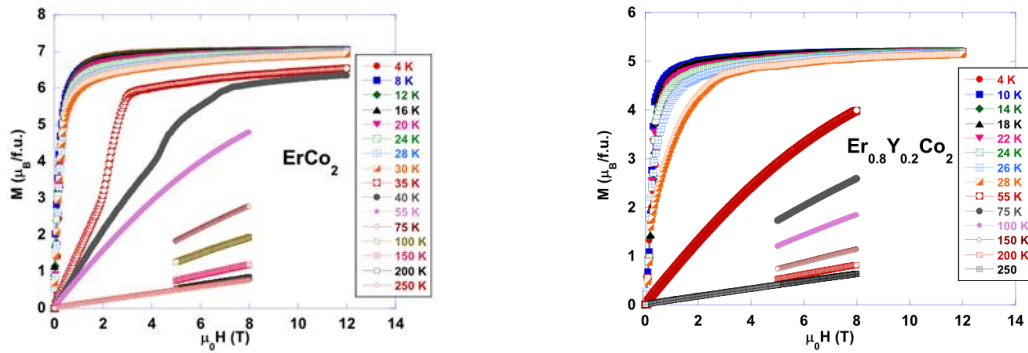


Fig.IV.1

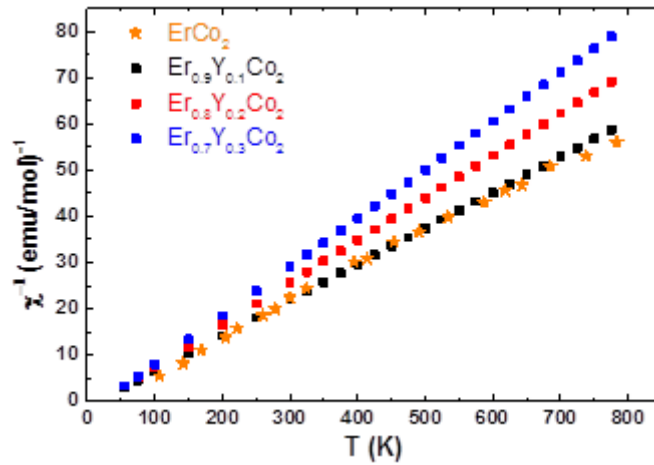


Fig.IV.2

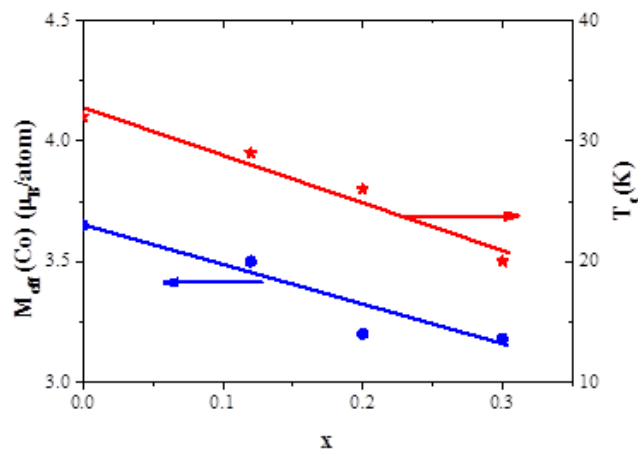


Fig.IV.3

The band structure calculations evidenced a smaller decrease of the cobalt moments as compared with experimentally determined values, when increasing Y content. The Er5d and Y4d bands are polarized, their magnetic moments decreasing in absolute magnitude as result of magnetic dilution effects. A constant ratio is obtained when the induced polarizations by short range exchange interactions, are divided by the magnetizations of the atoms situated in their first coordination shell  $(2.15 \pm 0.10) \cdot 10^{-2}$ . This value is nearly the same as that determined in  $RM_2$  ( $M = Fe, Co, Ni$ ) heavy rare-earths compounds.

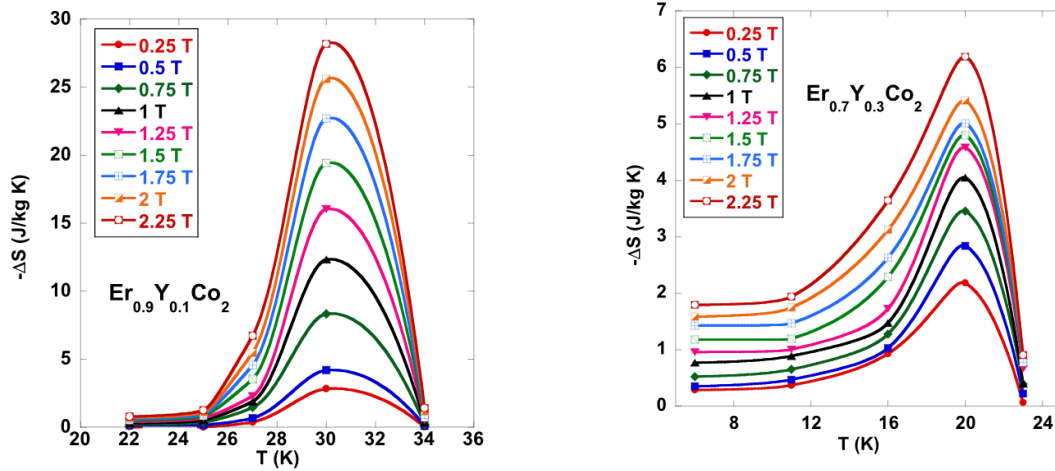


Fig.IV.4

The entropy changes,  $\Delta S$ , in  $Er_{1-x}Y_xCo_2$  compounds were computed from magnetization isotherms and successive values of the external fields. Higher entropy changes were evidenced in compounds with  $x = 0$  and  $0.1$ , which show first order magnetic transitions – Fig.IV.4. The relative cooling power,  $RCP(\Delta S)$  is of  $130 \text{ J/Kg}$  in  $Er_{0.9}Y_{0.1}Co_2$ , decreasing at  $42 \text{ J/kg}$  for sample with  $x = 0.2$ .

The cobalt magnetic behaviour in the above compounds, has been analysed in spin fluctuations model.

## IV.2 Exchange interactions in heavy rare-earth $RCo_2$ compounds

The exchange interactions in  $RCo_2$  compounds, at  $T < T_c$  are rather complex, essentially determining the cobalt moments. The exchange interactions between R and Co atoms takes place through the 4f-5d-3d path. The exchange interactions between cobalt atoms are of short range type. The R5d band polarizations,  $M_{5d}$ , are antiparallely oriented to cobalt moments. These values can be described by the relation – Fig.IV.5:

$$M_{5d} = M_{5d}(d) + \alpha G$$

where  $M_{5d}(d)$  is the induced polarization by R5d-Co3d short range exchange interaction,  $G$  is the De Gennes factor and the slope has a value of  $\alpha = 2.1 \cdot 10^{-2} \mu_B$ .

The exchange interactions at the level of unit cell are interdependent. The induced cobalt moments, by 4f-5d-3d exchange path, are modulated by Co3d-Co3d short range exchange interactions. The cobalt moments can be influenced by the magnetic dilution effects both at R and Co sites. Concomitantly, with the appearance of cobalt moment, an additional polarization,  $M_{5d(d)}$  is induced on R5d band by a reverse path, as depicted in inset of Fig.IV.5. Taking into account the complex and interdependent exchange interactions at the level of unit cell, this can be viewed as a “cluster” of magnetic interacting atoms, their lattice constant being the same as the correlation length determined by SANS experiments. Above, the Curie temperatures no magnetic ordered phase is present, as evidenced by linear dependences of magnetizations on the external field in  $\text{ErCo}_2$  – Fig. IV.6 or of cobalt and holmium moments in  $\text{HoCo}_2$  – Fig.IV.7.

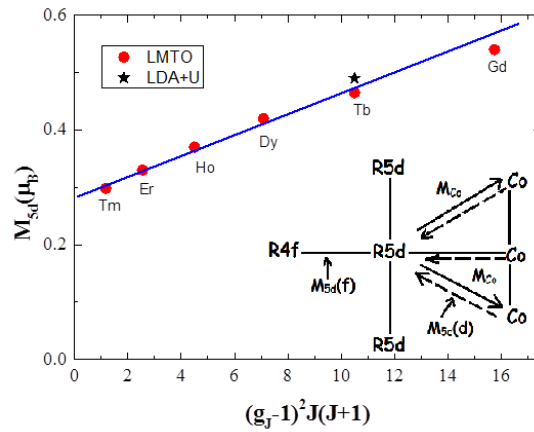


Fig.IV.5

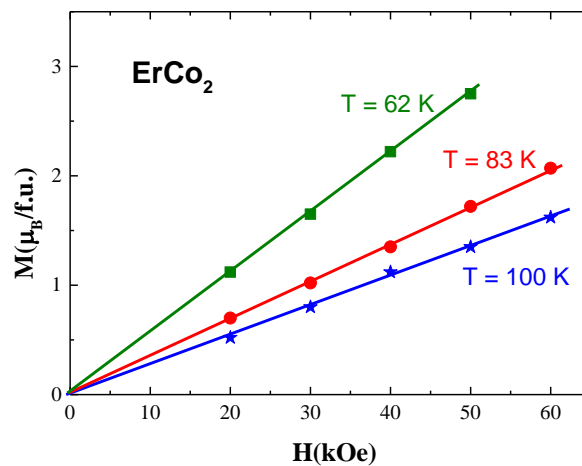


Fig.IV.6

Above  $T_c$ , in the presence of external fields, there are linear dependences of the cobalt moments on the rare-earth ones. This behaviour is not influenced by temperatures ( $40 \text{ K} \leq T \leq$

300 K) or external fields ( $10 \text{ kOe} \leq H \leq 57 \text{ kOe}$ ) – Fig. IV.8, supporting the presence only of a paramagnetic phase. The slopes of the above dependences,  $a = M_{\text{Co}}/M_{\text{R}}$  are dependent on rare-earth partner, following the same trend as the R5d band polarizations – Fig.IV.9.

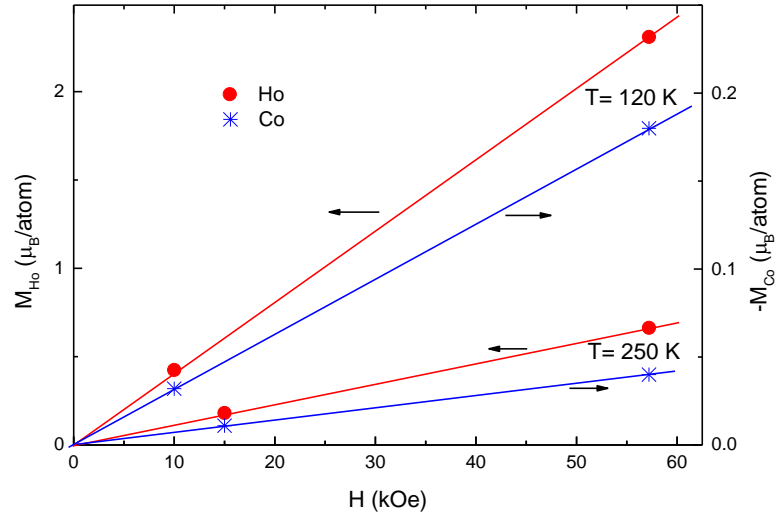


Fig.IV.7

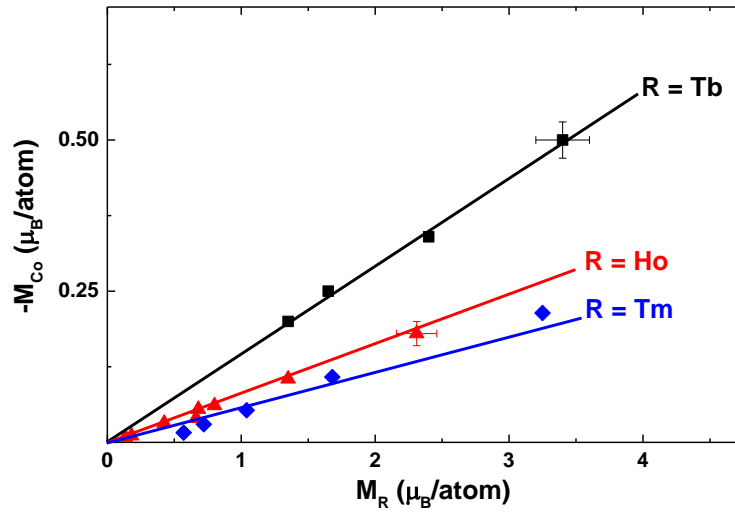


Fig.IV.8

The 4f-5d-3d exchange interactions, as well as those between cobalt atoms, are still present above the Curie temperatures, in a relative large temperature range. The exchange coupling are not enough to induce a magnetic ordering.

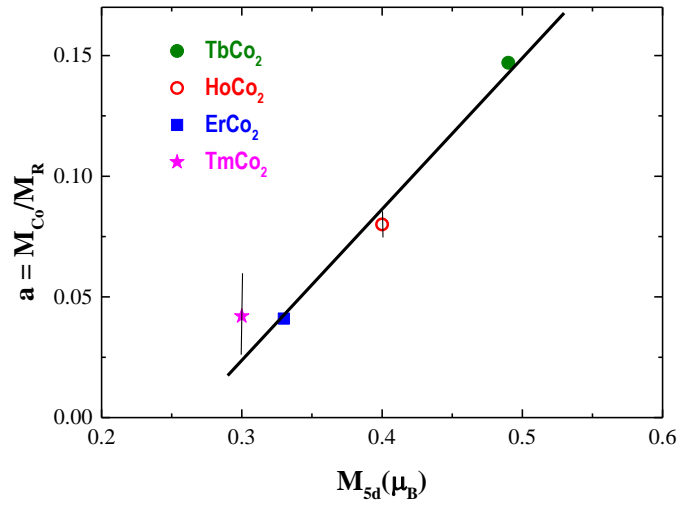


Fig.IV.9

The exchange field acting on cobalt atoms, at  $T > T_c$ , can induce only a very small additional cobalt magnetic moment. Even in the presence of an external field  $H = 57$  kOe, in addition to internal one, the estimated induced cobalt moment is below  $0.03 \mu_B$ .

The present data evidence that the “magnetic correlations” having  $\cong 7 \text{ \AA}$  correlation length, as evidenced by SANS experiments, can be associated with  $RCo_2$  unit cells ( $a \cong 7.2 \text{ \AA}$ ). Although the complex magnetic interactions are present at  $T > T_c$ , their intensities are not enough to induce a magnetic ordered state.

The magnetic arrangements of rare-earth and cobalt moments, in different temperature ranges, can be correlated with the temperature evolution of the energies involved in the system (exchange, thermal anisotropy as well as involving interactions of magnetic moments with external fields).

The scientific results obtained in analysing the magnetic properties of  $RCo_2$  have been published and accepted for publications.

IV.1. ***Magnetic and magnetocaloric properties of  $Er_{1-x}Y_xCo_2$  compounds with  $x \leq 0.3$***

**E.Burzo, I.Balasz, L. Chioncel**

*Rom. J. Phys.* 61, 6-7 (2016)

ISI Journal IF = 1.30

IV.2. ***Exchange interactions in heavy rare-earth  $RCo_2$  compounds***

**E.Burzo**

*J.Phys.: Conf. Series* (accepted to be published)

ISI journal

The following papers were presented at international conferences

IV.1. ***Exchange interactions in heavy rare-earth  $RCo_2$  compounds***

**E. Burzo,**

*International Conference on Neutron Scattering, Dubna, June 2016, p.18, Invited lecture*

**IV.2. *Magnetic and magnetocaloric properties of  $Er_{1-x}Y_xCo_2$  compounds***

**I. Balasz-Muresan, I.Balasz, L. Chioncel, E.Burzo**

*16<sup>th</sup> International Balkan Workshop on Applied Physics, July 2016, Constanta, Poster paper SIP73, p.74*

**IV.3. *Magnetic behaviour of  $RCo_2$  compounds, where  $R$  is a heavy rare-earth***

**E.Burzo,**

*11<sup>th</sup> International Conference on Physics of Advanced Materials, Sept., 2016, Invited Lecture, p.253*